Three-dimensional PTV Measurement of the Phase Relationship Between Coherent Structures and Dispersed Particles in a Turbulent Channel Flow

Yuji Suzuki, Motofumi Ikenoya, and Nobuhide Kasagi
Department of Mechanical Engineering, The University of Tokyo,
Hongo, Bunkyo-ku, Tokyo 113-8656, Japan

High-definition 3-D particle tracking velocimetry is successfully applied to simultaneous measurement of fluid and dispersed phase in a vertical turbulent water channel flow. Turbulent statistics are substantially modified by the solid particles having a diameter of 2-3 times the Kolmogorov length scale. The streamwise turbulent intensity of the fluid phase is significantly increased in the channel, whilst it is unchanged at $y^+<20$. In contrast, the wall-normal and spanwise components are increased in the whole cross-section. The quadrant analysis shows that the solid particles are densely distributed along the low-speed streaks, especially beneath the ejection event. The difference in traceability of particles to the ejection and sweep events should contribute to the particle agglomeration.

1. Introduction

Particle-laden turbulent flows are common in natural and industrial processes, and it is important to understand the mechanism of interaction between fluid and solid particles, especially in wall turbulence, from both engineering and environmental viewpoints.

Fessler et al. (1994) found from their experiment in a wind tunnel that the spatial distributions of solid particles are not uniform and concentrated in low vorticity regions. Kaftori et al. (1995) showed that particles are concentrated in the low-speed streaks in their horizontal turbulent channel. These particle clusters should play a important role in turbulence modification. Kulick et al. (1994) measured gas-solid two-phase flows in a vertical turbulent channel by using LDV. They found turbulent intensity is decreased when solid particles having a diameter smaller than the Kolmogorov length scale η are employed. Sato & Hishida (1996) made simultaneous measurements of fluid and dispersed phase with the aid of digital particle image velocimetry (DPIV), and found turbulent intensity is increased for larger particles (d_p~3η). Since their data are limited to the buffer and log regions, the near-wall behavior of turbulent statistics is unknown.

Recent development of numerical techniques enables us to carry out direct numerical simulations of particle-laden flows (e.g., Elghobashi & Truesdell, 1993; Pan & Banerjee, 1997; Boivin et al., 1998), and detailed information on turbulence modulation by particles were provided. However, the effect of various particle parameters on the turbulence modulation remains unclear, and there are still many discussions on the appropriate approach for the two-way coupling model between fluid and dispersed phase.

The objectives of the present study are to provide detailed statistics of both fluid and dispersed phase in a particle-laden turbulent channel flow, and to clarify the mutual interaction between near-wall coherent structures and solid particles. To do this, we apply a 3-D high-definition particle tracking velocimetry (hereafter, 3-D HDPTV) system to measure velocity vectors of solid and tracer particles simultaneously.

2. 3-D High-definition PTV system (3-D HDPTV)

With the aid of HD 3-D PTV, three velocity components of both fluid and dispersed phase are measured by tracking tracer and solid particles, respectively. The present technique is characterized by its use of three TV cameras that observe particles in a 3-D measurement volume from arbitrary viewing directions. It was originally developed by Nishino et al. (1989) and later improved by Sata & Kasagi (1992) for single-phase flow measurement.

The present measurement system is shown in Fig. 1. It consists of three high-definition CCD cameras (Sony, XCH-1125), three laser disk recorders (Sony, HDL-5800), a digital image processor (Nexus9000), and so on. The present image system has 1920x1024 pixels, which are about 8 times larger than that of the conventional NTSC system. Stroboscopes synchronized with the TV signal were employed for illumination. Images captured by each camera are recorded onto the laser disk recorder at 30 frames/s. Recorded images are then A/D converted and transferred to a workstation, by which further data reduction is carried out.

The tracer particles were chosen in such a way that their diameter is much less than that of the solid particles. Therefore,

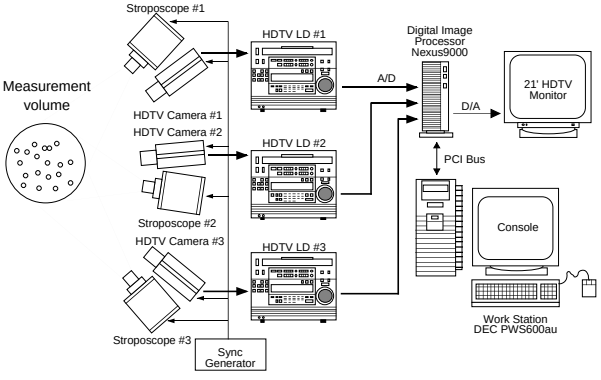

Figure 1: High-Definition 3-D PTV System.

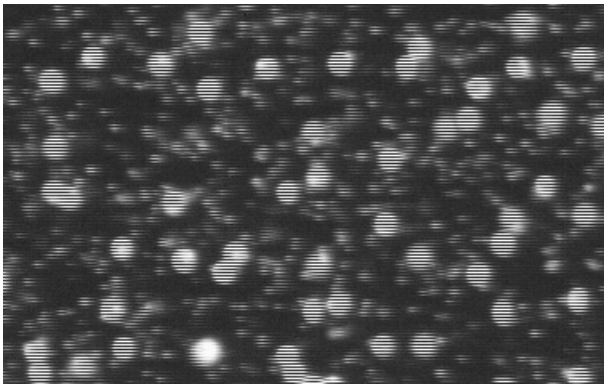

Figure 2: Typical raw image of solid and tracer particles (380 x 240 pixels). Note that two successive image field are overlaid in this image.

particle images can be easily grouped into two subsets, i.e., solid particles and tracer particles, depending on the size of the image. An example of raw image obtained in the present experiment described later is shown in Fig. 2. Instantaneous 3-D vectors of tracer and solid particles were obtained from successive four sets of particle images. Details of the particle tracking algorithm and the camera calibration procedure are found in Sata & Kasagi (1992) and Kasagi & Nishino (1992), respectively.

In order to evaluate the present measurement system, a computer simulation was made with the aid of a direct numerical simulation (DNS) database of particle-laden turbulent channel flow (Mizuya & Kasagi, 1998). The procedure is as follows: (i) generate solid and tracer particles randomly in space and calculate their trajectories by integrating their equation of motion, (ii) project 3-D particle position onto three virtual cameras, and generate numerically particle images, (iii) calculate photographic coordinates of each particle, (iv) reconstruct 3D position of particles and track each particle through the above mentioned procedure as used in the physical experiment. Parameters such as the flow condition, measurement volume, and viewing directions were given almost the same as those in the present experiment described later.

Figure 3(a) shows the number of particle trajectory N_v identified for the measurement of single phase flow as a function of the number of particle images N_I. In the range of N_I considered, N_v is increased monotonically, and up to 4000 instantaneous velocity vectors are obtained. Since the maximum value of N_v obtained with the NTSC system is about 600 (Ninomiya & Kasagi, 1993), we can expect 6-7 times more particle trajectories by using the present system.

Figure 3(b) shows N_v for particle-laden flow as a function of the number of solid particle images N_S. About 1600 and 650 vectors are simultaneously obtained from tracer and solid particles, respectively. Note that the turbulent statistics of fluid and particle motions obtained are in good agreement with the original DNS data.

3. Experimental facility and measurement condition

Measurements were carried out in a vertical channel (Fig. 4),

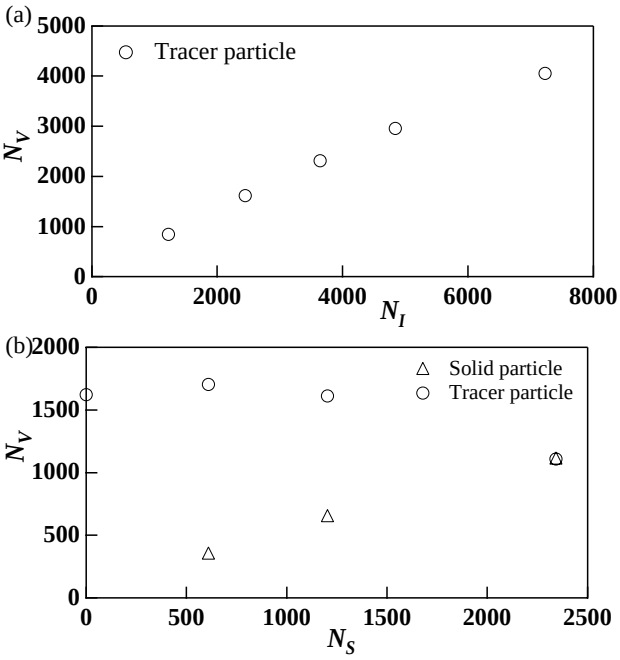

Figure 3: Dependence of yield of particle tracking on the number of particle images on an image plane. (a) Single phase flow, (b) Particle-laden flow.

where particle-laden water flows downward. The channel width H and height were 40 and 400 mm, respectively. The test section was located at $50H$ downstream of the inlet, where the flow was fully-developed. Solid and tracer particles were introduced uniformly into the flow field at the top of the channel by using a particle loading mechanism. Note that the time period in which the working fluid travels from the channel inlet to the test section is two orders of magnitude larger than the particle relaxation time, so that the particles should adapt sufficiently to the turbulent flow field. The test section and the camera setup are shown schematically in Fig. 5. A measuring volume was 50x25x25 (mm^3) in the streamwise (x), wall-normal (y), and spanwise (z) directions, respectively.

In the present study, two separate measurements were carried out. For the single-phase flow, only tracer particles were introduced into the flow, whilst both tracer and solid particles were fed for the particle-laden flow. The particle condition is summarized in Table. 1. Ceramic spherical beads (d_p~400μm, ρ_p/ρ_f=3.85) and Nylon 12 spherical particles (d_t~160μm, ρ_t/ρ_f=1.01) were used as the solid particles and flow tracers, respectively. The Kolmogorov length scale η was estimated to be 150 μm near the wall . Thus, d_t is almost the same as η, while d_p corresponds to about 2.7η. The volumetric concentration of solid particle is $3.2\text{x}10^{-4}$, where the substantial effect of the two-way coupling is expected (Elghobashi & Truesdell, 1993).

The centerline fluid velocity is 160 mm/s and 180 mm/s for the single-phase and the particle-laden flow, respectively. The Reynolds number based on the wall-friction velocity u_τ and the channel half-width was 172 for the single-phase flow, where u_τ was estimated by fitting the velocity distribution in the viscous sublayer to a profile predicted by a modified mixing length model

(McEligot, 1984).

Uncertainty intervals associated with the measured instantaneous velocities estimated at 95% coverage by the method of ANSI/ASME PTC 19.1(1986) are $0.06u_\tau$, $0.17u_\tau$, and $0.11u_\tau$ in the *x*, *y*, and *z* directions, respectively.

4. Results

Since the solid particles employed in the present study are opaque and have a light-diffusion surface, the viewing direction of each camera should be aligned with the incident light to obtain uniform image intensity of particles. Therefore, it is necessary to employ three stroboscopes placed close to individual cameras as shown in Fig. 5. However, this arrangement made particles outside of the measurement volume illuminated, so that the yield of velocity vectors is significantly decreased unlike the estimate shown in Fig 3 owing to the increase of overlapping particle images. For the single-phase flow, an average of 1200 instantaneous velocity vectors were obtained, whilst 270 and 150 vectors were simultaneously obtained for tracer particles and solid particles, respectively, in the case of the particle-laden flow. Note that, when semitransparent solid particles are employed, we can obtain much more instantaneous velocity vectors by using a single stroboscope to illuminate the measurement volume only.

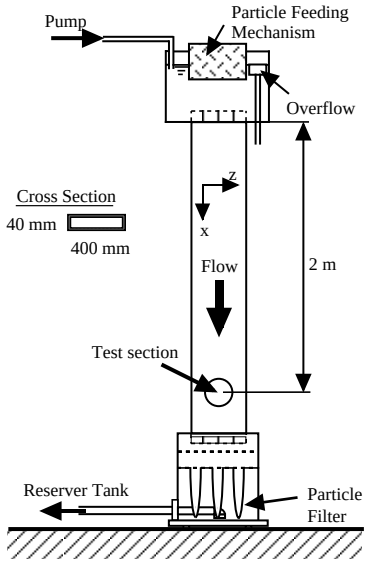

Figure 4: Turbulent water channel flow facility.

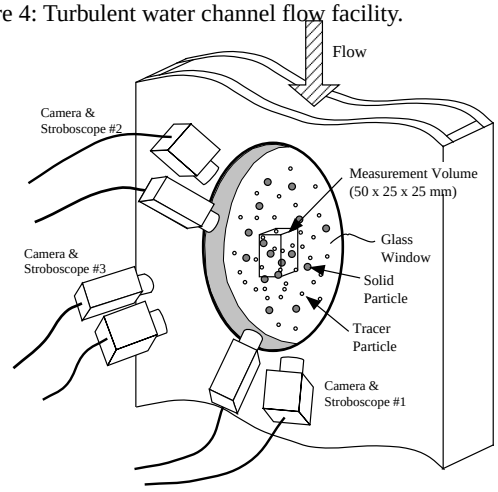

Figure 5: Test section and camera setup.

Table. 1: Particle Condition

	Diameter, d	Specific Density, ρ/ρ_f	Terminal Velocity, u_s	Time Constant, τ
Tracer Particle (Nylon 12)	150 - 180 μm	1.01	0.12 mm/s	1.45 ms $0.113\ \nu/u_\tau^2$
Solid Particle (Ceramic beads)	380 - 412 μm	3.85	87.2 mm/s	31.9 ms $2.49\ \nu/u_\tau^2$

Statistics were calculated as ensemble averages of velocity vectors grouped idepending on their distance to the wall. The wall-normal dimension of each data cell was set to be 0.2 mm.

Figure 6 shows the distribution of the number of velocity vectors obtained. The number of solid particles is significantly increased near the wall. Although the present data are not directly connected with the number density of particles, it is conjectured that solid particles are densely distributed near the wall due to the lift force toward the wall in the present experimental condition.

The streamwise mean velocity (U) distributions are shown in Fig. 7. The quantities are non-dimensionalized with the wall-friction velocity u_τ for each flow condition. The present result of the single-phase flow is in good agreement with the DNS data of

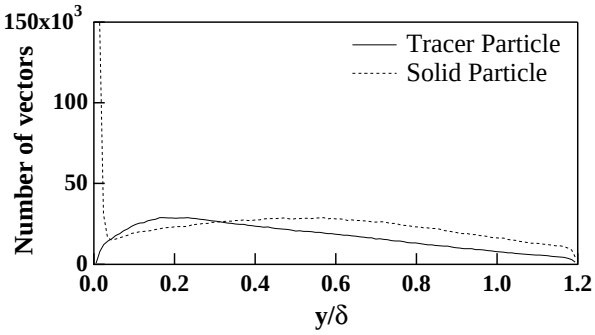

Figure 6: Number of vectors tracked.

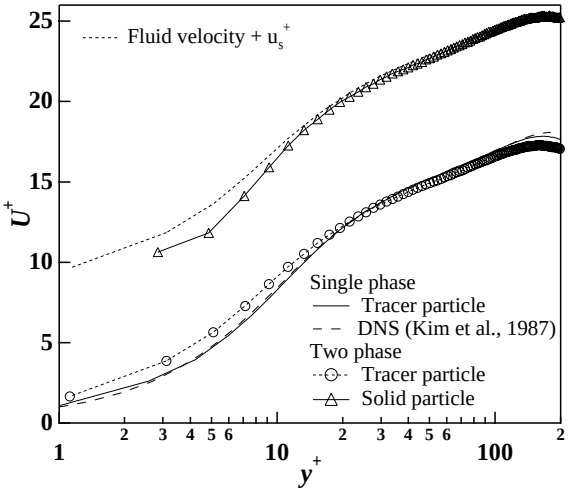

Figure 7: Mean streamwise velocity profiles of fluid and solid phase.

Kim et al. (1987). In the particle-laden flow, the fluid velocity in the viscous sublayer is slightly increased. The velocity gradient in the logarithmic region is slightly smaller than that of single phase, so that the Kárman constant should be modified by the presence of the dispersed phase. The mean velocity of solid particles is shifted upward due to the terminal velocity $u_s(=8u_\tau)$, while the difference is decreased at $y^+<10$. The present result is not in accordance with the LDV data of Kulick et al. (1994), which shows a significant slip velocity in the viscous sublayer, since the relaxation time of their glass and copper particles is 2-3 orders of magnitude larger than that of the present experiment.

The distributions of root-mean-square velocity fluctuations are shown in Fig. 8. In the single-phase flow, the rms values are again in good agreement with the DNS data of Kim et al. (1987). In the particle-laden flow, the streamwise component u_{rms} is unchanged at $y^+<20$, while it is significantly increased in the core of the channel and becomes as large as $2u_\tau$. On the other hand, the wall-normal and spanwise components are markedly increased in the whole region. Therefore, the anisotropy measure of the

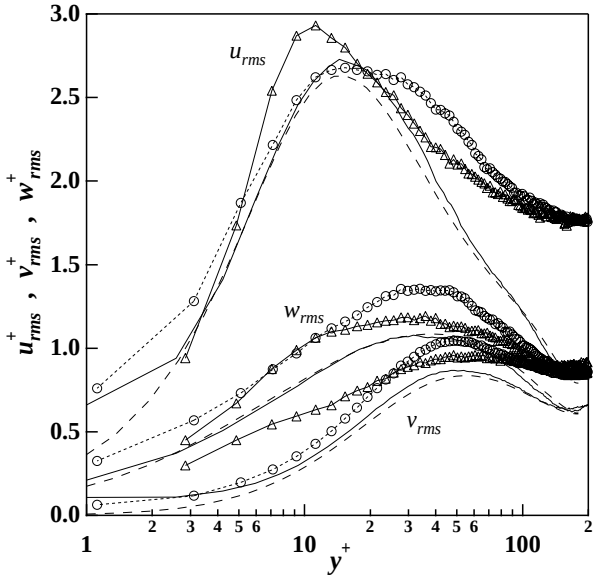

Figure 8: RMS velocity fluctuation profiles of fluid and solid phase. Keys as in Fig. 3.

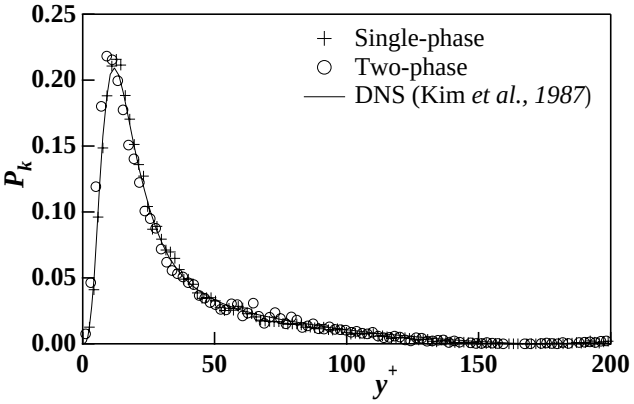

Figure 9: Distribution of production of the turbulent kinetic energy.

Reynolds normal stresses is decreased neat the wall, whilst it is increased in the core of the channel. Sato & Hishida (1996) also showed that u_{rms} is somewhat increased when glass beads ($d^+=5$, $\tau_p^+=3.5$) are employed, although the deviation of the rms values presently obtained over the single-phase flow data are much larger. The rms velocity fluctuations of solid particles are smaller than those of the fluid phase at $y^+>20$, while the streamwise and the wall-normal components become larger close to the wall. Note that the particle terminal velocity is varied among particles, since the solid particle used in the present study has a finite variance in diameter as shown in Table 1. However, the standard deviation in u_s is estimated as small as $0.2u_\tau$, and thus its effect on u_{rms} of solid particle should be negligible.

Figure 9 shows the turbulent production rate P_k due to the shear stress. It is clear that P_k is unchanged despite the substantial increase of the turbulent fluctuations at $y^+>20$. Although it is not shown here, the viscous and turbulent diffusion terms in the transport equation of the turbulent kinetic energy are also unchanged by the presence of the dispersed phase. Therefore, in the core of the channel, the turbulent energy should be directly generated in the wake behind the solid particles.

Figures 10 and 11 show contours of the ensemble-averaged streamwise velocity around solid particles in the *y*-*z* and *x*-*y* planes, respectively. Since the particle Reynolds number based on the terminal velocity u_s is about 33, the recirculating region downstream of particle is much less than d_p. However, the effect of solid particle is increased with increasing distance to the wall, and the accelerated region downstream persists more than 40 viscous length scale ($\sim 10d_p$) in the center of the channel. As shown in Figs. 10(c) and 11(c), the streamwise velocity upstream of the particle is also increased, so that it is conjectured that particle

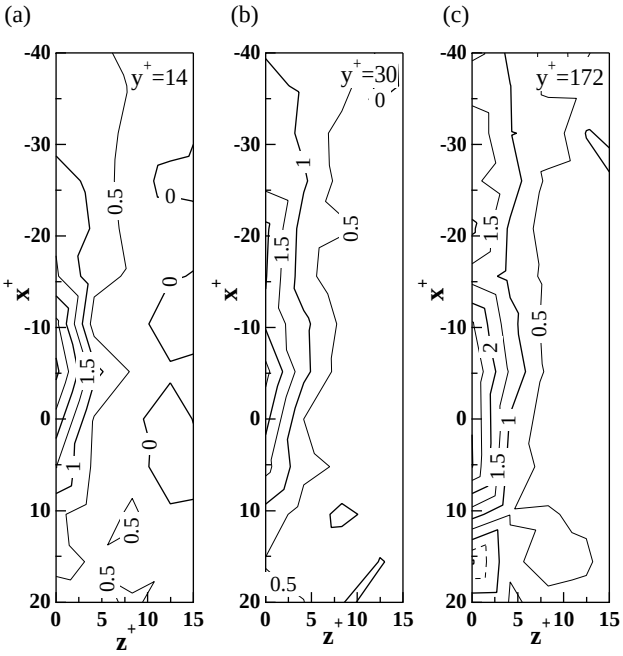

Figure 10: Contours of ensemble averaged streamwise velocity around solid particles in *x*-*z* plane. The location of solid particle is the orgin. (a) y^+=14, (b) y^+=30, (c) Channel centerline.

clusters are formed in the core of the channel.

Figures 12 and 13 show conditionally averaged quantities obtained by the quadrant analysis. The detection point was chosen at y^+ =14, and the threshold in the shear product was set as $0.5u_{rms}v_{rms}$. Figures 12(a) and 13(a) respectively show conditionally averaged fluid velocity vectors in the *y*-*z* plane for the ejection (Q2) and sweep (Q4) events. Since an additional condition for preserving the spanwise asymmetry (Choi & Guezennec, 1990) is not employed in the present analysis, a pair of counter-rotating quasi-streamwise vortices are clearly observed for both events. For the Q2 event, the streamwise velocity fluctuation is negative near the detection point (Fig. 12b), which corresponds to the low speed streaks. Underneath this region, the particle concentration is significantly large as shown in Fig. 12(c). This fact is in good agreement with the previous observation (e.g., Kaftori et al., 1995; Nino & Garcia, 1996) that solid particles having τ_p^+ ~4 are accumulated in the streaks. On the other hand, in the high-speed region associated with the Q4 event, the particle concentration becomes low (Figs. 13b, c).

Figure 14 shows the fractional occurrence of each quadrant event of the fluid and dispersed phase in the particle-laden flow. At y^+ >10, the fractional occurrence of the Q2 event for the solid particle is less than that of the fluid phase, while it is contrary for the Q4 event. Since the Q2 event is characterized by the multiple intense eruptions from single streak (Bogard & Tiederman, 1986), while the regions of the Q4 event are wider in the spanwise direction than those of the Q2 event (Robinson, 1991), the spatio-temporal scale of the Q2 event should be smaller than that of the Q4 event. Therefore, it is conjectured that solid particles can follow the fluid motion for the Q4 event but not for the Q2 event, and thus the difference of the traceability between the Q2 and Q4 events contribute to the agglomeration of particles into the low-speed streaks.

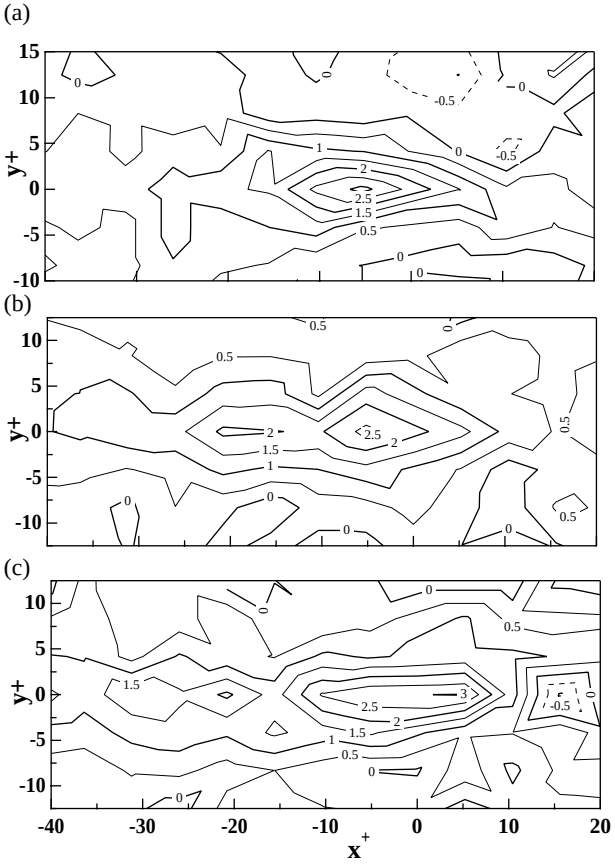

Figure 11: Contours of ensemble averaged streamwise velocity around solid particles in *x*-*y* plane. The location of solid particle is the orgin. (a) y^+=14, (b) y^+=30, (c) Channel centerline.

5. Conclusions

Three-dimensional high-definition particle tracking velocimetry is successfully applied to simultaneous measurement of fluid and dispersed phase in a turbulent water channel flow. Turbulent statistics of all three components are obtained as well as the conditional-averaged quantities with the aid of the quadrant analysis. The following conclusions are derived:

(1) Mean slip velocity of solid particles is almost the same as the terminal velocity except in the viscous sublayer.

(2) Streamwise turbulent intensity of the fluid phase is significantly increased in the core of the channel, while it is unchanged

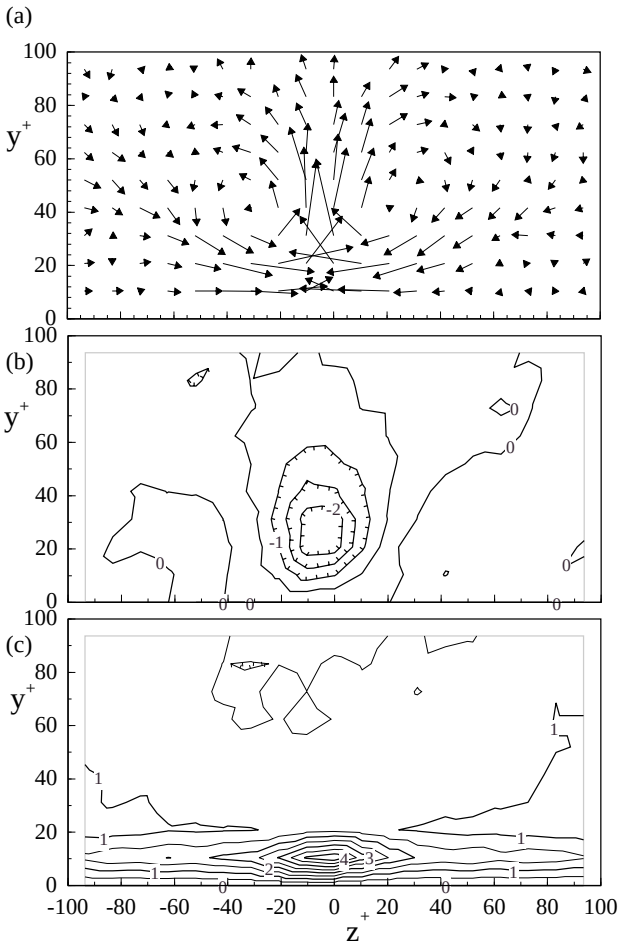

Figure 12: Conditional averaged quantities in the cross-stream plane associated with the ejection (Q2) event. (a) Velocity vectors, (b) Contours of streamwise velocity fluctuation, (c) Concentration of the solid particles.

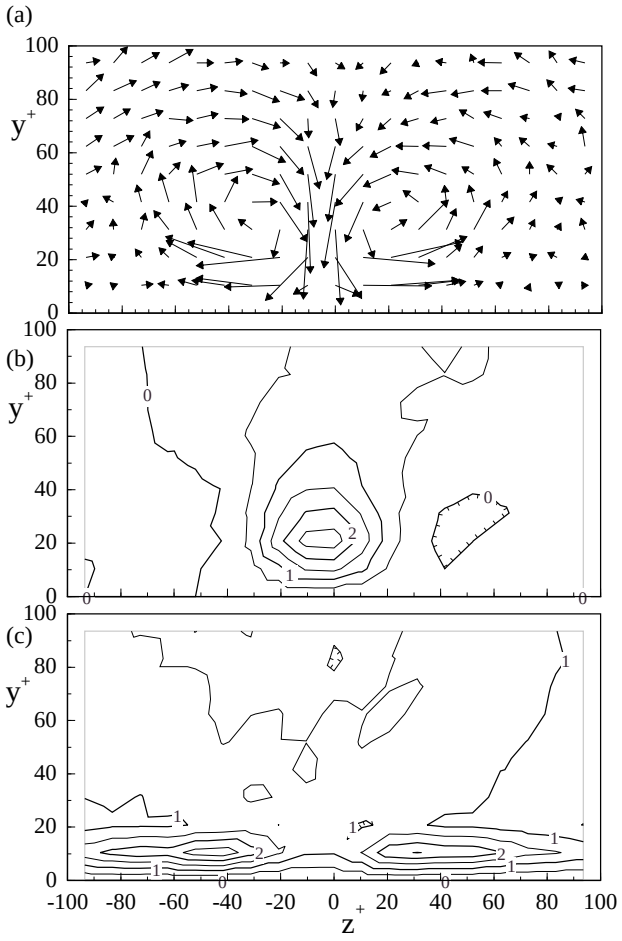

Figure 13: Conditional averaged quantities in the cross-stream plane associated with the sweep (Q4) event. (a) Velocity vectors, (b) Contours of streamwise velocity fluctuation, (c) Concentration of the solid particles.

at y^+<20. On the other hand, the wall-normal and the spanwise components are increased in the whole domain.

(3) Since turbulent production due to the shear stress is unchanged, the increase in turbulent intensity is attributed to the wake generation downstream of particles.

(4) The solid particles are densely distributed along the low-speed streaks, especially beneath the ejection event. A possible mechanism of the agglomeration is that the traceability of solid particles are different to the ejection and sweep events.

The authors are grateful to Mr. S. Ogino for his aid in laboratory work.

References

ANSI/ASME PTC 19.1-1985 (1987) Measurement uncertainty, supplement on instruments and apparatus, part 1

Boivin M; Simonin O; Squires KD (1998) Direct numerical simulation of turbulence modulation by particles in isotropic turbulence. J Fluid Mech 375: 235-263

Bogard DG; Tiederman WG (1986) Burst detection with single-point velocity measurements. J. Fluid Mech 162: 389-413

Choi WC; Guezennec YG (1990) On the asymmetry of structures in turbulent boundary layers. Phys Fluids A 2: 628-630

Elghobashi S; Truesdell GC (1993) On the two-way interaction between homogeneous turbulence and dispersed solid particles I: turbulence modification. Phys Fluids A 5: 1790-1801

Fessler JR; Kulick JD; Eaton JK (1994) Preferential concentration of heavy particles in a turbulent channel flow. Phys Fluids 6: 3742-3749

Kaftori D; Hetsroni G; Banerjee S (1995) Particle behavior in the turbulent boundary layer I. Motion, deposition, and entrainment. Phys Fluids 7: 1095-1106

Kasagi N; Nishino K (1992) Probing turbulence with three-dimensional particle-tracking velocimetry. Exp Thermal Fluids Sci 4: 601-610

Kim J; Moin P; Moser R (1987) Turbulence statistics in fully developed channel flow at low Reynolds number. J Fluid Mech 177: 133-166

Kulick JD; Fessler JR; Eaton JK (1994) Particle response and turbulence modification in fully developed channel flow. J Fluid Mech 277: 109-134

McEligot DM (1984) Measurement of wall shear stress in accelerating turbulent flows. Max-Planck-Institüt für Strömungs-forschung, Bericht 109, Göttingen, Germany

Mizuya T; Kasagi N (1998) Numerical analysis of particle motion in turbulent channel flow. Proc 3rd Int Conf Multiphase Flow, in CD-ROM p632.pdf, Lyon

Nino Y; Garcia MH (1996) Experiments on particle-turbulence interactions in the near-wall region of an open channel flow: implications for sediment transport. J Fluid Mech 326 285-319

Ninomiya N; Kasagi N (1993) Measurement of the Reynolds Stress Budgets in an Axisymmetric Free Jet with the Aid of Three-Dimensional Particle Tracking Velocimetry. Proc. 9th Symp on Turbulent Shear Flows 6.1.1-6.1.6, Kyoto

Nishino K; Kasagi N; Hirata M (1989) Three-dimensional particle tracking velocimetry based on automated digital image processing. ASME J Fluid Eng 111: 384-391

Pan Y; Benerjee S (1997) Numerical investigation of the effects of large particles on wall-turbulence. Phys Fluids 9: 3786-3807

Robinson SK (1991) The kinematics of turbulent boundary layer structure. NASA TM 103859

Sata Y; Kasagi N (1992) Improvement towards high measurement resolution in three-dimensional particle tracking velocimetry. Proc 6th Int Symp. Flow Vis: 792-796, Yokohama

Sato Y; Hishida K (1996) Transport process of turbulent energy in particle-laden turbulent flow. Int J Heat & Fluid Flow 17: 202-210

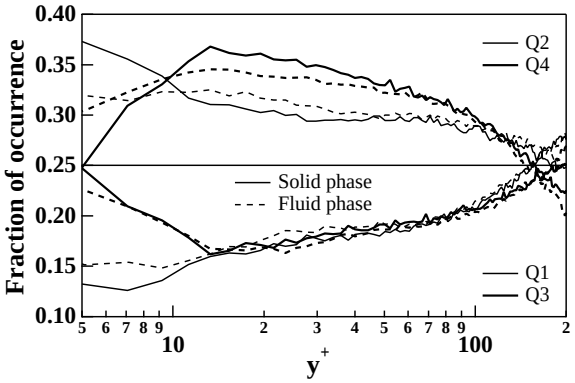

Figure 14: Fraction of occurrence of each quadrant event.